Affinity and Valence Impact the Extent and Symmetry of Phase Separation of Multivalent Proteins

Saroj Kumar Nandi,[1,2] Daniel Österle,[3] Meta Heidenreich,[3] Emmanuel D. Levy,[3] and Samuel A. Safran[1]
[1]*Department of Chemical and Biological Physics, Weizmann Institute of Science, Rehovot 7610001, Israel*
[2]*Tata Institute of Fundamental Research, Hyderabad 500046, India*
[3]*Department of Chemical and Structural Biology, Weizmann Institute of Science, Rehovot 7610001, Israel*

(Received 24 October 2019; revised 7 July 2022; accepted 11 August 2022; published 15 September 2022)

Biomolecular self-assembly spatially segregates proteins with a limited number of binding sites (valence) into condensates that coexist with a dilute phase. We develop a many-body lattice model for a three-component system of proteins with fixed valence in a solvent. We compare the predictions of the model to experimental phase diagrams that we measure *in vivo*, which allows us to vary specifically a binding site's affinity and valency. We find that the extent of phase separation varies exponentially with affinity and increases with valency. Valency alone determines the symmetry of the phase diagram.

DOI: 10.1103/PhysRevLett.129.128102

Introduction.—Protein self-assembly plays a central role both in health and disease [1]. Aberrant protein assembly is associated with neurodegenerative diseases such as Alzheimer's or Huntington's [2,3], type-II diabetes [4], and others. Conversely, protein self-assembly into biomolecular condensates can spatially localize biochemical processes in membraneless, mesoscale compartments [5,6]. These biomolecular condensates (BMCs) can comprise ribonucleic acids, nucleic acids, and various proteins [5–8]. Examples of such BMCs include germline granules [9,10], stress (responsive) granules [11–16], and chromatin-bound condensates [17]. BMCs also display crucial regulatory roles in various biological processes [1,5,18] such as cell differentiation [19,20], centrosome assembly [21,22], reaction kinetics [23], noise buffering [24–26], or metabolic control [27]. Thus, general theoretical frameworks that enable conceptualization and prediction of the behavior of BMC systems are critical for comparison with experiments to foster their control. These include understanding the concentrations, molecular interactions, and temperature [5,18,28,29] under which biomolecules condensate instead of remaining dispersed, or assessing whether the formation of a BMC is a quasiequilibrium process [30] or whether it is driven by biochemical reactions [21,22].

Quantitative analyses of *in vivo* cellular condensates are difficult owing to the fact that one does not know all the molecular species involved or the interactions among them. Such uncertainty limits the ability to quantitatively predict the properties of phase separation of cellular condensates. For example, BMCs often comprise intrinsically disordered proteins [5] for which the structural valency (number of binding sites available per molecule), the effective valency (number of sites that are sterically, simultaneously accessible for intermolecular contacts) and the interaction energy (affinity) between binding sites are typically unknown. In that respect, synthetic systems help bridge this gap, as their parameters are known by design. Indeed, the use of synthetic systems *in vitro* enabled understanding the impact of protein concentration, as well as interaction affinity on phase separation [23,31]. We have developed a unique, synthetic system based on interacting dimers and tetramers that enforces intermolecular contacts, so that the structural valency is equal to the effective valency [32]. The modularity of this system also allows one to vary the valency parameter—for example, replacing tetramers with hexamers, and changing the bond affinity, as we demonstrate in this Letter.

Additionally, BMCs fundamentally differ from systems studied in physics and physical chemistry, where one usually considers isotropically interacting, small molecule mixtures. In contrast, biomolecules are large, and in many cases, interactions are constrained by their geometry and the number and position of binding sites at their surface. Simple models with nonspecific interactions predict phase separation with a critical volume fraction of the order of $1/2$ [33,34]. In contrast, for polymeric systems, Flory-Huggins theory [35] predicts a critical concentration that scales as $N^{-1/2}$, where N is the polymerization index. For large N, the system phase separates at very low polymer volume fractions with a fractal-like polymeric ensemble. In addition, for branched polymers, the classical theory of gelation by Flory and Stockmayer [36–38] gives the percolation threshold of the network, a geometric property. However, our interest here is on the thermodynamic phase separation that leads to condensate formation. Reference [39] presents the effects of varying multivalency on both phase separation and percolation. The latter, in particular, highlights that valence is a critical parameter. Our theory complements the existing approaches listed

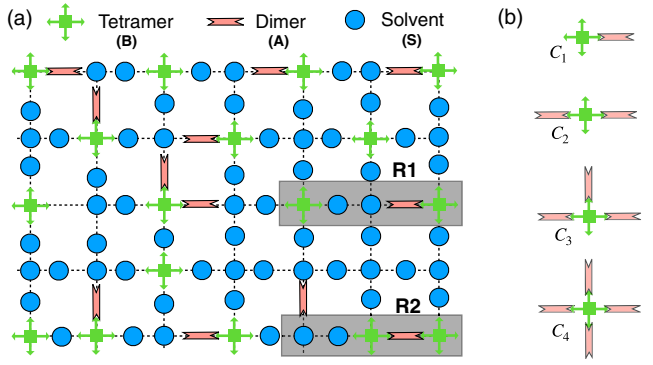

FIG. 1. Schematic description of the lattice model for a solution of tetramers, dimers, and solvent. (a) Lattice model for the system on a square lattice. Regions R1 and R2 show the same particles in two different configurations: the configuration in R2 has higher enthalpy owing to satisfied interactions between A and B and a lower entropy as other configurations of A and B are restricted by the interaction. The configuration in R1 has lower enthalpy and higher entropy than R2. (b) Four possible complexes when the B molecules are tetramers.

above: we focus on the primary physical mechanisms relating phase separation to finite multivalency of rigid proteins. Progress along this direction has come from molecular-dynamics simulations of patchy particles [40,41], the extension of Wertheim theory [42–45], and lattice-based Monte Carlo simulations of model biological proteins [46–48]. In this Letter, we develop a relatively simple lattice model that automatically includes the excluded volume effect and the multibody nature of finite valence. This makes the theory amenable to analytical treatment and facilitates comparison with experiments on the extent of phase separation as a function of affinity and valence.

Our focus here is the phase separation into concentrated and dilute regions in a three-component system of a solvent and two proteins: one of which is divalent (dimer) and another with a valence larger than two (multimer). The multimers interact among themselves via the dimers, which link two multimers as schematically shown in Fig. 1. The geometric design of the proteins prevents intramolecular binding, i.e., where two sites of a dimer bind on the same multimer. Experimentally, we genetically encode such a pair of proteins and monitor their expression and phase separation in yeast cells, as described in Ref. [32]. Briefly, the dimer and multimer each consists of three structured domains fused by flexible linkers: the first domain is a fluorescent reporter, the second confers multivalence by homo-oligomerization, and the third mediates the affinity or interaction strength (IS) between the dimer and the multimer. Uniquely, both IS and the multimer valency can be modulated by exchanging the IS-domain or multivalent-domain with another exhibiting the desired property. The dimer and tetramer are coexpressed in the cytoplasm of yeast cells and undergo phase separation at high enough concentrations. Protein concentration in the dilute phase is quantified by fluorescence microscopy and is compared with our theory. Theoretically, we predict the phase diagram topology and symmetry (the axis of maximum phase separation) for the association of such multimers linked (or not) by dimers. We find that the phase boundaries enclosing the coexisting regions form closed loops and crucially depend on the valence and relative affinity, IS, between the dimers and multimers (Fig. 2). We, therefore, focus on the phase diagrams as a function of the dimer and multimer concentrations at various interaction strengths (Fig. 2). For these coexistence curves, the valence determines the symmetry that depends on the multimer-dimer ratio [Fig. 3(b)]; this is different from closed-loop phase diagrams in the temperature-solute concentration plane for hydrogen-bonding systems [49,50]. In addition, our theory predicts that the minima (minimum distance from the origin), Δ, of the phase diagrams vary exponentially with interaction strength, which is in agreement with experimental data [Figs. 2(c)–2(f)]. We then elucidate the role of multivalency in phase separation and how valency affects the rate of decrease of the distance to the origin Δ with IS [Fig. 3(c)]. Finally, we show within the theory and the experiment that phase separation becomes more effective (i.e., phase boundaries cover a larger region of the concentration space) at higher valence for a fixed interaction strength [Figs. 3(d)–3(f)].

Theoretical model.—We formulate a statistical mechanical description of the system of multimers and dimers, which we solve within a mean-field approximation. Since the focus of the experiments is on the topology and symmetry of the phase diagrams as a global function of the two concentrations at fixed temperature, the corrections to mean-field theory are important only near the critical points and therefore are not of interest here. Instead, we focus on the experimentally important parameters of compositions, valence, and interaction strengths. We designate the dimers by A and the multimers by B. The proteins in the experiments are designed so that A and B interact as lock and key [32,51]. Additionally, two interaction sites of A cannot bend to interact with two sites of the *same* B molecule due to the rigidity of A. Therefore, phase separation proceeds through intermolecular associations between A and B.

For concreteness, we first consider a particular example: a dimer and a tetramer being the A and B particles, respectively, and the rest of the system is considered as a uniform (mostly aqueous, in the case of a cell) solvent S. From the experiment, we find the phase separation to be strongest (i.e., the concentration difference between the two coexisting phases is largest) at the stoichiometric ratio of interaction sites (volume fraction of molecules multiplied by their valence) of A and B. To elucidate this within our mean-field theory, we consider a lattice model where the A molecules occupy only the bonds and the B molecules occupy only the sites of the lattice. Solvent molecules, S,

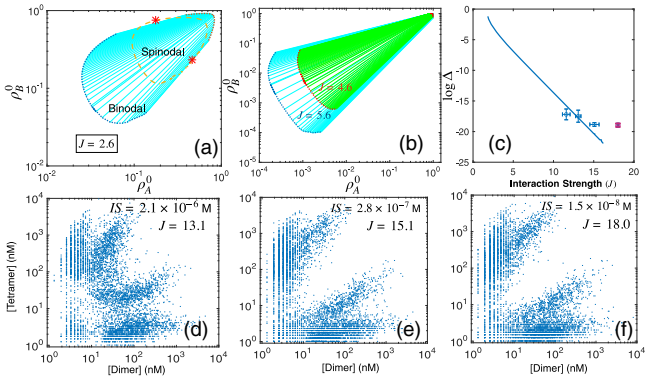

FIG. 2. (a) Phase diagram for a solution of tetramers, dimers, and solvent. The dotted line denotes the binodal and the end points of the tie lines (in light blue) are the concentrations of the concentrated (dashed) and dilute (dotted) phases. The yellow dashed line is the spinodal that gives the limit of metastability. The two red stars denote the two critical points where the tie line length vanishes and the two coexisting phases become identical. (b) Binodal for solutions of tetramers, dimers, and solvent at two different values of the interaction strength, J, show stronger phase separation (larger area of the two-phase region and larger differences in concentrations of the two coexisting phases) at larger J. (c) The minimum distance Δ of the phase boundary from the origin as a function of interaction strength J. The line is the theory and the symbols (with error bars) are experimental data. We note that the data point for the highest interaction strength (purple) overestimates Δ because the corresponding concentrations of A and B in the dilute phase reach a value below the detection limit of the microscope. (d)–(f) Experimental phase diagrams for the dimer-tetramer system with different interaction strengths (affinities) ($J = -\log(IS)$ in units of k_BT).

can occupy either the bonds or sites as schematically shown in Fig. 1(a). N_s and N_b denote the total number of sites and bonds, respectively. Since the B molecules have four interaction sites ($q = 4$) each, we consider a square lattice, where $N_b = 2N_s$; to treat other valences, q, we use different lattices (see Supplemental Material (SM) [52], Sec. V). The system contains a total of N_0^A A molecules and N_B^0 B molecules. Since the lattice is fully occupied, conservation dictates that there must be $(2N_s - N_A^0)$ S molecules on the bonds and $(N_s - N_B^0)$ on the sites.

Modeling the experimental phase diagrams requires the inclusion of many-body interactions to account for the finite valency, even in mean-field theory [53,54]. To do so, we proceed in two separate stages: first, the A and B molecules associate with each other forming complexes, and second, the complexes interact among themselves as well as with the free B molecules (i.e., those not associated with any A) leading to phase separation. To simplify the problem and obtain physical insight, we use a mean-field approximation where the complexes interact with the average concentration of B molecules. For the particular case of tetramers and dimers, there can be four different complexes: C_i with $i = 1, 2, 3, 4$, where C_i denotes a configuration with i A molecules associated with one B molecule as schematically shown in Fig. 1(b).

To illustrate the physical origin of the phase separation, consider the two shaded regions $R1$ and $R2$ in Fig. 1(a): they both contain the same number of particles: one A, two B, and two S. When the attractive interaction dominates, the configuration in $R2$ has lower free energy compared to that in $R1$; in contrast, when entropy dominates, the arrangement in $R1$ has lower free energy than that in $R2$. In equilibrium, the system configuration is that which minimizes its free energy: When the enthalpy term dominates, it favors $R2$, and the system phase separates; on the other hand, when the entropy term dominates, it favors $R1$, and the system remains in a homogeneous, single phase.

After the complexes have formed, the dimensionless concentration of free A molecules (the fraction of bonds occupied by uncomplexed A molecules) is $\rho_A = N_A/N_b$, where N_A is the number of free A molecules. Similarly, $\rho_B = N_B/N_s$ is the dimensionless concentration of free B molecules. This particular normalization uses the effective concentrations of the interaction sites (i.e., actual concentrations multiplied by valence), which is the quantity that we also use for analysis of the experiments. The effective concentrations of the total (overall) A and B interaction sites are ρ_A^0 and ρ_B^0, respectively, and the concentrations of the ith complex are γ_i. Then, the total free energy (see SM [52], Sec. II, for details), f, per site, in units of k_BT, where k_B is the Boltzmann constant and T, the temperature, is

$$\begin{aligned} f = {} & 2\rho_A \ln\rho_A + \rho_B \ln\rho_B + 2(1-\rho_A^0)\ln(1-\rho_A^0) \\ & + (1-\rho_B^0)\ln(1-\rho_B^0) + \gamma_1 \ln(4\gamma_1) + \gamma_2 \ln(6\gamma_2) \\ & + \gamma_3 \ln(4\gamma_3) + \gamma_4 \ln\gamma_4 - J(\gamma_1 + 2\gamma_2 + 3\gamma_3 + 4\gamma_4) \\ & - (J - J_{BB})\rho_B^0(\gamma_1 + 2\gamma_2 + 3\gamma_3 + 4\gamma_4), \end{aligned} \tag{1}$$

where the product iJ is the gain in binding energy (in units of k_BT) due to the formation of C_i. J_{BB} is a parameter governing the change in interaction when both sides of the dimer, compared to only one of its sides, is attached to the corresponding site on the B molecules. Here, we consider $J_{BB} = 0$ and comment on nonzero J_{BB} in the SM [52], Sec. IX. Note that we have treated the solvent on the sites and the bonds as two different states, since the volumes occupied by A and B molecules can be different.

Modeling the effect of interaction strength on phase separation.—Conservation of the A and B molecules respectively implies that $\rho_A = \rho_A^0 - (\gamma_1 - 2\gamma_2 - 3\gamma_3 - 4\gamma_4)/2$ and $\rho_B = \rho_B^0 - \gamma_1 - \gamma_2 - \gamma_3 - \gamma_4$, where the γ_i are the concentrations of the complexes. For a given interaction strength J, we first minimize f with respect to γ_is; this leads to four equations that we solve simultaneously to obtain the γ_is in terms of ρ_A^0 and ρ_B^0, which then allows us to calculate the phase diagrams (see SM [52], Sec. II). The phase diagrams are functions of the interaction strength J, ρ_A^0

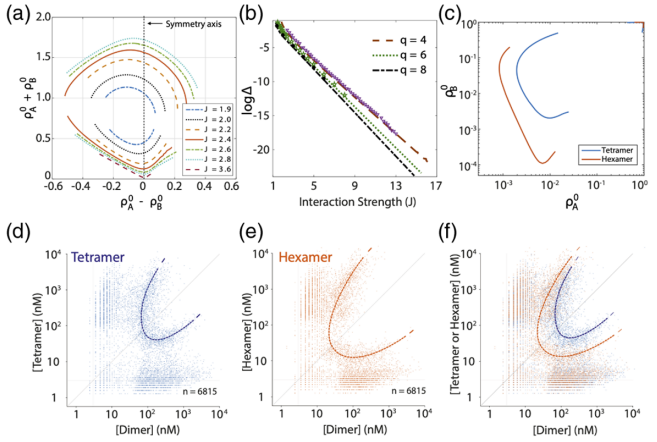

FIG. 3. (a) The symmetry axis of the phase diagrams for phase separation of tetramers and dimers lies along the zero of the abscissa for asymptotically large J. This shows that phase separation is strongest at the stoichiometric ratio (of the effective concentrations). (b) Comparison of the value of the minimal concentration, Δ, obtained from the full model (points) and simplified model (lines) along the symmetry axis. (c) Theoretical phase diagram for both tetramers and dimers and hexamers and dimers, both with $J = 4.0$ shows stronger phase separation for the hexamers. (d)–(f) Experimental phase diagrams for the same interaction strength and different valence (d) Phase diagram for a dimer-tetramer system (e) Phase diagram for a dimer-hexamer system. (f) Experimental data from panels (d) and (e) are overlaid. Axes correspond to concentration of interaction sites and dotted lines are approximate phase boundaries.

and ρ_B^0, and therefore are three-dimensional. We plot the phase diagrams in the two-dimensional plane of the given effective concentrations, ρ_A^0 and ρ_B^0, at a fixed value of J. There is no phase separation at small values of J; as J increases and crosses a certain value (depending on valence), phase separation occurs. We find a closed-loop phase diagram with two critical points as shown for $J = 2.6$ in Fig. 2(a). The outer boundary, marked by the dotted line, is the binodal, and the dashed line is the spinodal. Phase separation occurs inside the binodal region where dense (red) and dilute (blue) regions coexist in equilibrium, whereas outside this boundary, the system remains homogeneous. The two stars mark the critical points where the concentrations of dense and dilute regions become identical. The lines connecting the dense and the dilute regions are the tie lines, whose end points are the effective concentrations of two coexisting regions. If the interaction strengths and overall concentrations are such that the effective concentrations are within the spinodal region, the uniform, mixed state is unstable, and phase separation occurs via spinodal decomposition along the tie lines. On the other hand, if the system lies between the spinodal and the binodal regions, phase separation proceeds through nucleation and growth [33,39,55].

Figure 2(b) shows the binodal phase diagrams for the tetramer-dimer system at two different values of J; increasing J leads to more effective phase separation (as defined above). For a quantitative comparison of theory and experiment, we define Δ, the minimum distance of the dilute region of the binodal from the origin, as a function of different J and the corresponding experimentally varied affinity. In a two-component system, Δ decreases exponentially with J when $J \gg 1$ (see SM [52], Sec. VI); we expect and observe a similar behavior for the three-component system. We plot Δ derived from the numerical solution of the theory (line) and from the experiment (symbols; see SM [52], Sec. I) in Fig. 2(c). The experimental uncertainty in both the affinity (corresponding to the interaction strength, J) and the measured effective concentrations are shown in the figure. Note that the concentrations at the largest affinities in experiments are at the limits of our experimental resolution. The agreement in Fig. 2(c) is close given the experimental uncertainties. We also show the experimental phase diagrams at three different affinities (interaction strengths IS, measured in units of M, where $J = -\log(IS)$ in units of k_BT). The points in Figs. 2(d)–2(f) are the effective concentrations of interaction sites of dimers and tetramers for cells that do not exhibit a visible condensate in them; thus, the data from the many cells with different protein concentrations depicts the part of the binodal that delineates the dilute phase [32].

Although the theoretical phase diagram is a closed loop, a quantitative measurement of the concentration in the dense phase is challenging due to the limited axial resolution of the microscope, inner filter effects, and foster energy transfer. Therefore, we compared only the dilute region of the measured phase diagrams with the theory. In the experimental system, A and B interact with an affinity on the order of 100 nM or $\sim 15 k_BT$ [32]. The numerical solution of the theory at such affinities is impractically slow (see SM [52], Sec. VII) and we did not calculate the entire phase diagram. However, we discuss in the SM [52] and show in Fig. 3 that the extreme regions of the phase diagram (those that connect largest tie lines) can be calculated even for large values of J. We saw in Fig. 2 that the shapes of the phase diagrams for the dilute region, and the trend with increasing J, are similar to the situation at smaller values of J. (See, however, SM [52], Sec. IV, for a comment on the difference of the shapes of phase diagrams in theory and experiments.) When the affinity is high, the system will use more A molecules to associate the B molecules, as schematically shown in Fig. 1(a). As shown in the SM [52] (Fig. S3), when the affinity of A to B is weak, the likelihood of complex formation is low, and most of A molecules are free; whereas, for high affinity, the probability is high, and most of the A molecules are incorporated into complexes. These complexes then interact with the free B particles or other complexes to yield the dense phase.

We expect maximal phase separation when the effective concentrations of interaction sites for the two species are equal. To test this hypothesis, we plot the phase diagrams

for a mixture of dimers and tetramers at several values of J as functions of $\rho_A^0 - \rho_B^0$ vs $\rho_A^0 + \rho_B^0$ in Fig. 3(a). As J increases, we expect the symmetry line, i.e., the tie line of maximal phase separation, to lie on the zero of the abscissa, which we indeed observe [Fig. 3(a)]. If stoichiometry determines the maximal extent of phase separation, Δ should lie along this symmetry axis. To test this hypothesis, we approximate $\rho_A^0 = \rho_B^0$ and solve the phase diagrams along this symmetry axis (see SM [52], Sec. VIII). Δ obtained using this simple approximation agrees well with the numerical results of the complete theory [Fig. 3(b)].

Effect of valency.—We now discuss the role of multivalency. For concreteness, we consider two different systems: tetramers or hexamers, both with dimers and solvent (see SM [52], Sec. V). All other parameters being equal, we find that the system with hexameric B molecules shows a larger region of phase separation, compared with tetramers, as shown in Fig. 3(c) for $J = 4.0$. To compare the theory with experiments, we measured the phase diagrams for both systems: tetramers or hexamers with dimers; the phase diagrams are shown in Figs. 3(d)–3(f) and experimental details are given in the SM [52]. Consistent with theory, phase separation is more effective for the hexamers than the tetramers at a given interaction strength, and a similar effect was observed using three structurally distinct hexameric scaffolds (Fig. S1 and SM [52], Sec. I). Note that the trivial factor that accounts for a larger number of interaction sites per multimer is accounted for in these plots as we consider concentrations of interaction sites, not concentrations of B molecules. The system with larger valence shows stronger phase separation due to the availability of more complexes, which increases the interaction energy per particle. Smaller values of Δ with increasing multivalency q at a fixed J [Fig. 3(c)] are also consistent with the experimental results.

In summary, we have presented a simple theory that predicts phase separation in a three-component system of multivalent proteins where one of the components is dimeric and the other has a higher valence. While we have shown the results for tetramers and hexamers, and octamers, the theoretical approach can be extended to other systems. The theory is motivated by and compared with experiments on cytoplasmic phase separation within yeast cells where the phase separating proteins are synthetic and foreign to those cells [32]. Since these proteins are not expected to interact with the intrinsic proteins of the cells, the experimental system allows quantitative control over the interaction strengths and valency of the system compared with cellular protein condensates, which can have any number of additional unknown components. In most cases of intracellular phase separation, the knowledge on protein-protein interactions is incomplete; our experimental system, along with the analytical theory, should be viewed as a step toward a quantitative understanding of the phase separation process *in vivo*.

S. K. N. would like to thank Ohad Cohen, Dan Deviri, Timon Idema, and A. Radhakrishnan for discussions and the Koshland Foundation for funding through a fellowship. S. K. N. also acknowledges intramural funds at TIFR Hyderabad from the Department of Atomic Energy (DAE), India, under Project Identification Number RTI 4007 and SERB for grant via SRG/2021/002014. S. A. S. is grateful for the support of the Weizmann-Curie grant, the Krenter and Perlman Family Foundations, the Volkswagen foundation, and a Katz-Krenter Center grant. E. D. L. acknowledges support by the Israel Science Foundation (1452/18), by the European Research Council (ERC) under the European Union's Horizon 2020 research and innovation programme (Grant Agreement No. 819318), by a research grant from A.-M. Boucher, by research grants from the Estelle Funk Foundation, the Estate of Fannie Sherr, the Estate of Albert Delighter, the Merle S. Cahn Foundation, Mrs. Mildred S. Gosden, the Estate of Elizabeth Wachsman, and the Arnold Bortman Family Foundation.

[1] A. Zbinden, M. Pérez-Berlanga, P. D. Rossi, and M. Polymenidou, Dev. Cell **55**, 45 (2020).
[2] T. R. Peskett, F. Rau, J. O'Driscoll, R. Patani, A. R. Lowe, and H. R. Saibil, Mol. Cell **70**, 588 (2018).
[3] S. Ghosh, T. B. Sil, S. Dolai, and K. Garai, FEBS J. **286**, 4737 (2019).
[4] L. Pytowski, C. F. Lee, A. C. Foley, D. J. Vaux, and L. Jean, Proc. Natl. Acad. Sci. U.S.A. **117**, 12050 (2020).
[5] S. F. Banani, H. O. Lee, A. A. Hyman, and M. K. Rosen, Nat. Rev. Mol. Cell Biol. **18**, 285 (2017).
[6] A. S. Lyon, W. B. Peeples, and M. K. Rosen, Nat. Rev. Mol. Cell Biol. **22**, 215 (2021).
[7] Y. Shin and C. P. Brangwynne, Science **357**, eaaf4382 (2017).
[8] J. Berry, C. P. Brangwynne, and M. Haataja, Rep. Prog. Phys. **81**, 046601 (2018).
[9] J. Smith, D. Calidas, H. Schmidt, T. Lu, D. Rasoloson, and G. Seydoux, eLife **5**, e21337 (2016).
[10] S. Saha, C. A. Weber, M. Nousch, O. Adame-Arana, C. Hoege, M. Y. Hein, E. Osborne-Nishimura, J. Mahamid, M. Jahnel, L. Jawerth, A. Pozniakovski, C. R. Eckmann, F. Jülicher, and A. A. Hyman, Cell **166**, 1572 (2016).
[11] D. S. W. Protter and R. Parker, Trends Cell Biol. **26**, 668 (2016).
[12] M. M. Kucherenko and H. R. Shcherbata, Nat. Commun. **9**, 312 (2018).
[13] A. K. Jayabalan, A. Sanchez, R. Y. Park, S. P. Yoon, G.-Y. Kang, J.-H. Baek, P. Anderson, Y. Kee, and T. Ohn, Nat. Commun. **7**, 12125 (2016).
[14] S. J. Seguin, F. F. Morelli, J. Vinet, D. Amore, S. D. Biasi, A. Poletti, D. C. Rubinsztein, and S. Carra, Cell Death Differ. **21**, 1838 (2014).
[15] A. Molliex, J. Temirov, J. Lee, M. Coughlin, A. P. Kanagaraj, H. J. Kim, T. Mittag, and J. P. Taylor, Cell **163**, 123 (2015).

[16] J. A. Riback, C. D. Katanski, J. L. Kear-Scott, E. V. Pilipenko, A. E. Rojek, T. R. Sosnick, and D. A. Drummond, Cell **168**, 1028 (2017).
[17] A. R. Strom, A. V. Emelyanov, M. Mir, D. V. Fyodorov, X. Darzacq, and G. H. Karpen, Nature (London) **547**, 241 (2017).
[18] D. M. Mitrea and R. W. Kriwacki, Cell Commun. Signaling **14**, 1 (2016).
[19] X. Liu, J. Shen, L. Xie, Z. Wei, C. Wong, Y. Li, X. Zheng, P. Li, and Y. Song, Dev. Cell **52**, 277 (2020).
[20] F. G. Quiroz, V. F. Fiore, J. Levorse, L. Polak, E. Wong, H. A. Pasolli, and E. Fuchs, Science **367**, eaax9554 (2020).
[21] D. Zwicker, M. Decker, S. Jaensch, A. A. Hyman, and F. Jülicher, Proc. Natl. Acad. Sci. U.S.A. **111**, E2636 (2014).
[22] D. Zwicker, A. A. Hyman, and F. Jülicher, Phys. Rev. E **92**, 012317 (2015).
[23] P. Li, S. Banjade, H.-C. Cheng, S. Kim, B. Chen, L. Guo, M. Llaguno, J. V. Hollingsworth, D. S. King, S. F. Banani, P. S. Russo, Q.-X. Jiang, B. T. Nixon, and M. K. Rosen, Nature (London) **483**, 336 (2012).
[24] A. Klosin, F. Oltsch, T. Harmon, A. Honigmann, F. Jülicher, A. A. Hyman, and C. Zechner, Science **367**, 464 (2020).
[25] T. Stoeger, N. Battich, and L. Pelkmans, Cell **164**, 1151 (2016).
[26] D. Deviri and S. A. Safran, Proc. Natl. Acad. Sci. U.S.A. **118**, e2100099118 (2021).
[27] M. Prouteau and R. Loewith, Biomolecules **8**, 160 (2018).
[28] C. P. Brangwynne, C. R. Eckmann, D. S. Courson, A. Rybarska, C. Hoege, J. Gharakhani, and F. J. A. A. Hyman, Science **324**, 1729 (2009).
[29] M. Feric, N. Vaidya, T. S. Harmon, D. M. Mitrea, L. Zhu, T. M. Richardson, R. W. Kriwacki, R. V. Pappu, and C. P. Brangwynne, Cell **165**, 1686 (2016).
[30] A. A. Hyman, C. A. Weber, and F. Jülicher, Annu. Rev. Cell Dev. Biol. **30**, 39 (2014).
[31] S. Alberti, A. Gladfelter, and T. Mittag, Cell **176**, 419 (2019).
[32] M. Heidenreich, J. Georgeson, E. Locatelli, L. Rovigatti, S. K. Nandi, A. Steinberg, Y. Nadav, E. Shimoni, S. Safran, J. P. K. Doye, and E. D. Levy, Nat. Chem. Biol. **16**, 939 (2020).
[33] S. A. Safran, *Statistical Thermodynamics of Surfaces, Interfaces, and Membranes* (Addison-Wesley Publishing Company, Reading, MA, 1994).
[34] K. A. Dill and S. Bromberg, *Molecular Driving Forces: Statistical Thermodynamics in Chemistry and Biology* (Garland Science, London and New York, 2003).
[35] P. G. D. Gennes, *Introduction to Polymer Dynamics* (Cambridge University Press, Cambridge, England, 1990).
[36] P. J. Flory, *Principles of Polymer Chemistry* (Cornel University Press, Ithaca, 1953).
[37] W. H. Stockmayer, J. Chem. Phys. **11**, 45 (1943).
[38] W. H. Stockmayer, J. Chem. Phys. **12**, 125 (1944).
[39] A. Zilman, J. Kieffer, F. Molino, G. Porte, and S. A. Safran, Phys. Rev. Lett. **91**, 015901 (2003).
[40] E. Bianchi, J. Largo, P. Tartaglia, E. Zaccarelli, and F. Sciortino, Phys. Rev. Lett. **97**, 168301 (2006).
[41] F. Smallenburg, L. Leibler, and F. Sciortino, Phys. Rev. Lett. **111**, 188002 (2013).
[42] M. S. Wertheim, J. Stat. Phys. **35**, 19 (1984).
[43] M. S. Wertheim, J. Stat. Phys. **35**, 35 (1984).
[44] M. S. Wertheim, J. Stat. Phys. **42**, 459 (1986).
[45] M. S. Wertheim, J. Stat. Phys. **42**, 477 (1986).
[46] T. S. Harmon, A. S. Holehouse, M. K. Rosen, and R. V. Pappu, eLife **6**, e30294 (2017).
[47] T. S. Harmon, A. S. Holehouse, and R. V. Pappu, New J. Phys. **20**, 045002 (2018).
[48] J.-M. Choi, F. Dar, and R. V. Pappu, BioarXiv (2019), 10.1101/611095.
[49] J. C. Wheeler and G. R. Andersen, J. Chem. Phys. **73**, 5778 (1980).
[50] J. S. Walker and C. A. Vause, Phys. Lett. **79A**, 421 (1980).
[51] W. Li, S. J. Hamill, A. M. Hemmings, G. R. Moore, R. James, and C. Kleanthous, Biochemistry **37**, 11771 (1998).
[52] See Supplemental Material at http://link.aps.org/supplemental/10.1103/PhysRevLett.129.128102 for summary of the experimental system and the details of the theoretical calculations.
[53] A. Radhakrishnan and H. M. McConnel, Biophys. J. **77**, 1507 (1999).
[54] A. Radhakrishnan and H. McConnel, Proc. Natl. Acad. of Sci. U.S.A. **102**, 12662 (2005).
[55] A. J. Bray, Adv. Phys. **43**, 357 (1994).